Volume 3 | Number 16 | 28 April 2015 | Pages 8217–8906

Journal of Materials Chemistry A

Materials for energy and sustainability

www.rsc.org/MaterialsA

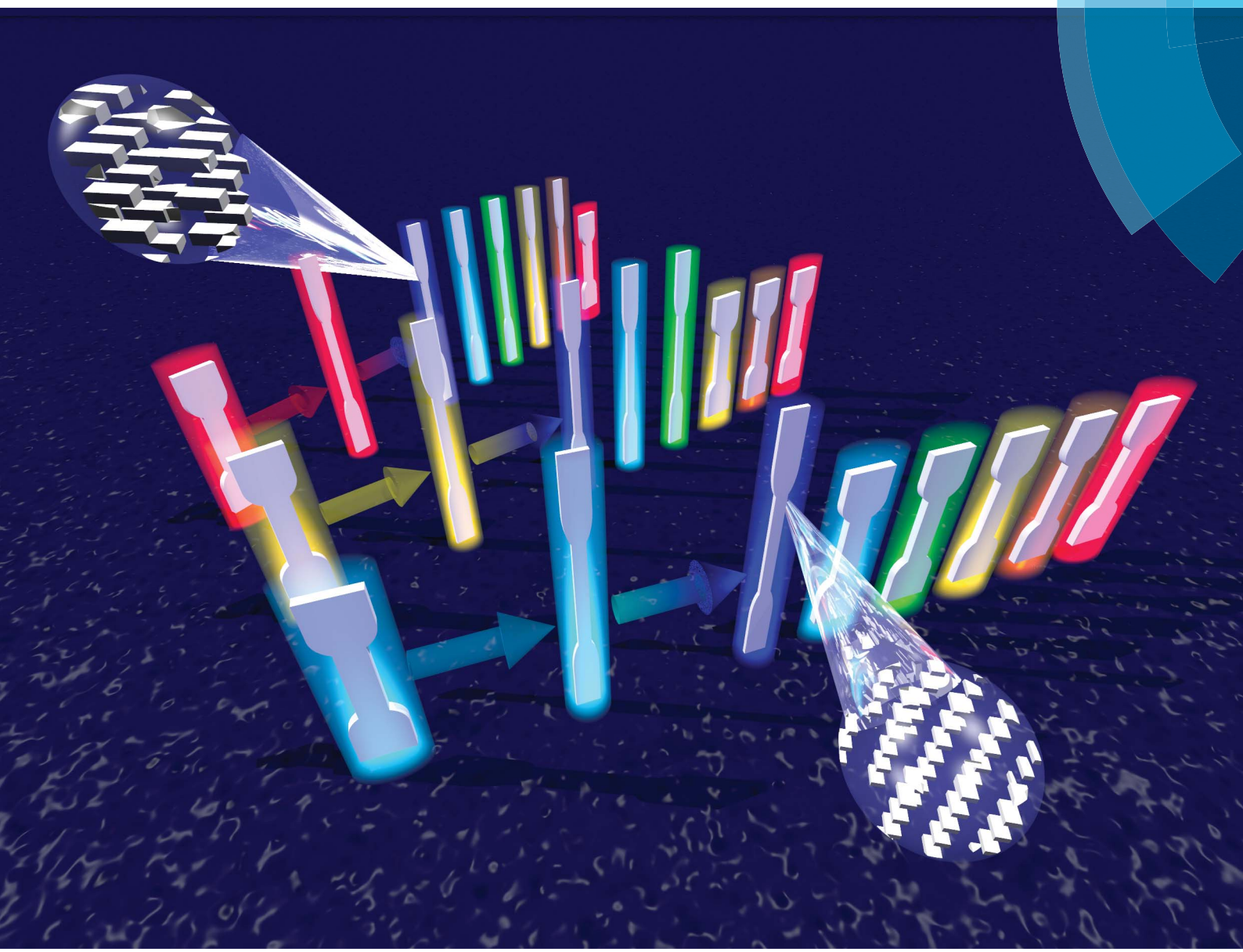

ISSN 2050-7488

ROYAL SOCIETY OF CHEMISTRY

PAPER

Andreas Lendlein *et al.*

Nanostructural changes in crystallizable controlling units determine the temperature-memory of polymers

Journal of Materials Chemistry A

PAPER

View Article Online
View Journal | View Issue

Cite this: J. Mater. Chem. A, 2015, 3, 8284

Nanostructural changes in crystallizable controlling units determine the temperature-memory of polymers†

Ulrich Nöchel,‡[a] Chaganti Srinivasa Reddy,‡§[a] Ke Wang,¶[a] Jing Cui,‖[a] Ivo Zizak,[b] Marc Behl,[a] Karl Kratz[a] and Andreas Lendlein*[ac]

Received 1st December 2014
Accepted 10th February 2015

DOI: 10.1039/c4ta06586g

www.rsc.org/MaterialsA

Temperature-memory polymers remember the temperature, where they were deformed recently, enabled by broad thermal transitions. In this study, we explored a series of crosslinked poly[ethylene-*co*-(vinyl acetate)] networks (cPEVAs) comprising crystallizable polyethylene (PE) controlling units exhibiting a pronounced temperature-memory effect (TME) between 16 and 99 °C related to a broad melting transition (~100 °C). The nanostructural changes in such cPEVAs during programming and activation of the TME were analyzed *via in situ* X-ray scattering and specific annealing experiments. Different contributions to the mechanism of memorizing high or low deformation temperatures (T_{deform}) were observed in cPEVA, which can be associated to the average PE crystal sizes. At high deformation temperatures (>50 °C), newly formed PE crystals, which are established during cooling when fixing the temporary shape, dominated the TME mechanism. In contrast, at low T_{deform} (<50 °C), corresponding to a cold drawing scenario, the deformation led preferably to a disruption of existing large crystals into smaller ones, which then fix the temporary shape upon cooling. The observed mechanism of memorizing a deformation temperature might enable the prediction of the TME behavior and the knowledge based design of other TMPs with crystallizable controlling units.

1. Introduction

Thermo-sensitive polymer networks exhibiting a temperature-memory effect (TME)[1–8] typically exhibit a broad thermal transition ΔT_{trans}[9] or two overlapping thermal transitions, which could also exhibit multi-shape effects.[10–12] Temperature-memory polymers (TMPs) can memorize the temperature T_{deform} within ΔT_{trans}, where they have been deformed during programming. The original shape of the programmed TMP is recalled when response temperatures T_{sw} are exceeded, whereby T_{sw} are equal to or above T_{deform}. The temperature interval ΔT_{trans}, which can be either a glass (T_g) or melting (T_m) transition, can be considered as an ensemble of individual sharp transitions ($T_{trans,i}$), whereby each single sharp transition can be utilized as reversible physical crosslinks for fixation of the temporary shape. In this context, first theoretical model approaches have recently been introduced for the description of amorphous TMPs.[2,13,14] Still, it is relevant to understand and experimentally confirm the mechanistic aspects of TME in polymers with crystallizable controlling units. One example for polymers having a broad ΔT_m and showing excellent temperature-memory properties over a temperature interval of up to 90 °C is crosslinked poly[ethylene-*co*-(vinyl acetate)] (cPEVA) comprising amorphous vinyl acetate (VA) segments and crystallizable polyethylene (PE) segments.[4] The broad ΔT_m in cPEVA is a result of the sequence structure of the copolymer and in particular the distribution of PE segment lengths, which are related to the thickness of the crystalline lamellae. The broadness of ΔT_m in cPEVA can be influenced by either the weight fraction of VA co-monomer or the crosslink density of the polymer network.

We hypothesized that the TME capability of cPEVA is enabled by specific nanostructures of the crystals, which remember the temperature of the deformation. Several contributions might influence the crystallizable controlling units when a temperature-memory creation procedure (TMCP) is applied, which includes a deformation step at certain T_{deform} within ΔT_m. First, the temperature (T_{deform}) prior deformation

[a]Institute of Biomaterial Science, Helmholtz-Zentrum Geesthacht, Kantstr. 55, 14513 Teltow, Germany. E-mail: andreas.lendlein@hzg.de
[b]Helmholtz-Zentrum Berlin, Institute for Nanometer Optics and Technology, Albert-Einstein-Str. 15, 12489 Berlin, Germany
[c]Institute of Chemistry, University Potsdam, Karl-Liebknecht-Str. 24-25, 14476 Potsdam, Germany

† Electronic supplementary information (ESI) available. See DOI: 10.1039/c4ta06586g

‡ Authors contributed equally.

§ Present address: The Centre for Research on Adaptive Nanostructures and Nanodevices and School of Physics, Trinity College Dublin, Dublin 2, Ireland.

¶ Present address: Institute of Materials Physics and Technology, Hamburg University of Technology, 21073 Hamburg, Germany.

‖ Present address: BASF Advanced Chemicals Co. Ltd, 200137 Shanghai, China.

could be considered as an isothermal treatment, permitting the variation of crystal dimensions. Second, the deformation step could lead into a rearrangement of the crystal structure (*e.g.* orientation of crystals) and third, the contribution of the cooling step when fixing the temporary shape will influence the nanostructure responsible for memorizing different T_{deform}s. These changes of the semi-crystalline nanostructure would be caused both by the temperature within the melting range and the deformation to the temporary shape.

In this study, we explored the nanostructural changes during temperature-memory programming and recovery for a series of cPEVAs with regard to the contribution of temperature treatment by means of specific annealing experiments as well as DSC analysis, the influence of the deformation step during temperature-memory creation procedure at different temperatures, and the contribution of the cooling step on the formed semi-crystalline nanostructure *via in situ* X-ray scattering techniques (small- and wide-angle X-ray scattering SAXS/WAXS). In this way, the effect of applying different T_{deform}s on the nanostructure of PE crystalline domains in programmed cPEVAs and therefore on the TME mechanism could be revealed.

In the following we describe the thermomechanical characterization of the cPEVA copolymer networks. Their nanostructure is explored by SAXS and WAXS and compared to theoretical dimensions. The thermal contribution to the TME is investigated by annealing experiments of non-deformed samples and analyzed by DSC. The contribution of the mechanical deformation at T_{deform} and the contribution of the cooling step to changes of the nanostructure of the crystallizable controlling units are investigated *in situ* by SAXS and WAXS. Finally, mechanisms at high and low T_{deform} are deduced from these experiments and temperature dependent pathways for the TME are presented.

2. Experimental

2.1. Materials

Poly[ethylene-*co*-(vinyl acetate)]s (DuPont, Wilmington, USA) with vinyl acetate contents of 18 wt% and 28 wt% (data of supplier) and the thermosensitive initiator dicumyl peroxide (DCP) (Sigma-Aldrich, Taufkirchen, Germany) were used as received. Copolymer networks were prepared as described in reference,[15] *i.e.*, PEVAs were mixed with 0.5, 1, or 2 wt% DCP in a twin-screw extruder (EuroPrismLab, Thermo Fisher Scientific, MA, USA) at 110 °C and 50 rpm. The obtained PEVA/DCP blends were compression molded into films with 1 mm thickness at 200 °C at 20 bar for 25 min.

2.2. Thermogravimetric analysis (TGA)

TGA measurements were carried out on a TGA 209 (NETZSCH, Selb, Germany) in the temperature range from 25 °C to 700 °C with a heating rate of 20 K min^{-1}. The composition of cPEVA was analyzed according to the weight loss of acetic acid groups observed in the temperature range from 300 °C to 410 °C,[16] where the vinyl acetate weight content (VAC) was calculated by eqn (1).

$$\text{VAC} = \frac{w_1\left(\frac{M_w(\text{VA})}{M_w(-\text{COOCH}_3)}\right)}{w} \times 100 \quad (1)$$

here w_1 is the weight loss attributed to the deacetylation of VA segments in the temperature range from 300 °C to 410 °C and w is total weight of cPEVA samples. M_w (VA) is the molar mass of VA and M_w (–COOCH_3) the molar mass of the acetic acid groups. The sample ID cPEVAxx denotes the VAC as determined by TGA.

2.3. ^{1}H-NMR spectroscopy

^{1}H-NMR spectroscopy was recorded at 25 °C on a 500 MHz Advance spectrometer (Bruker, Karlsruhe, Germany) using tetramethylsilane (TMS) as internal standard. Experiments were performed at 500 MHz (^{1}H) resonance frequency with the spectral width of 10 000 Hz. Samples were dissolved in toluene-d_8 at 50 °C for 18 h prior to the measurements. The assigned chemical shifts were: (a) –COOCH_3– (methylene protons near the carboxyl group, $\delta = 1.8$ ppm), (b) –CH– (methylene protons near the carboxyl group, $\delta = 5.0$ ppm), and (c) –CH_2– (linear methylene protons, $\delta = 1.3$–1.6 ppm) (see ESI Fig. S1†).

The ^{1}H-NMR data were used for calculation of the theoretical average segment length of PE sequences using the formula $n_0 = 1 + 2F_e/F_v$, where n_0 is the segment length, F_e the ethylene mole fraction, and F_v the VA mole fraction.[17]

2.4. Swelling experiments

The gel content (G) was determined by gravimetric relation of the non-extracted reaction product to the purified polymer network. The purification procedure consisted of extraction with toluene at 50 °C for 24 h, removing all un-reacted fractions and drying the samples at 50 °C under vacuum until constant weight was reached (eqn (2)). cPEVAs purified by extraction were used for determination of equilibrium swelling Q in toluene (eqn (3)):

$$G = \frac{m_{\text{extracted}}}{m_{\text{non-extracted}}} \times 100 \quad (2)$$

$$Q = \left[1 + \frac{\rho_{\text{polymer}}}{\rho_{\text{solvent}}}\left(\frac{m_{\text{swollen}}}{m_{\text{dried}}} - 1\right)\right] \times 100 \quad (3)$$

here m_{sw} and m_d represent the swollen and dry weights of the networks, ρ_{polymer} and ρ_{solvent} are the specific densities of the network and solvent respectively.

2.5. Differential scanning calorimetry (DSC)

DSC measurements were performed on a DSC 204 Phoenix (NETZSCH, Selb, Germany) applying a heating–cooling–heating cycle at heating and cooling rates of 10 K min^{-1} between −100 and 150 °C. The melting temperatures of cPEVAs were obtained from the second heating run. Furthermore, the melting enthalpy related weight crystallinity (w_c) of cPEVAs was calculated from DSC endothermic curves obtained from second heating according to eqn (4).

$$w_c = \frac{\Delta H_m}{\Delta H_m{}^{100}} \times 100 \quad (4)$$

here ΔH_m is the melting enthalpy, representing the area of the melting peak, and $\Delta H_m{}^{100}$ is the specific melting enthalpy for a 100% crystalline PE segment (287.3 J g^{-1}).[18]

2.6. Annealing experiments

For annealing the copolymer networks, samples were placed in the thermo-chamber of the tensile tester and were heated to 90 °C and then cooled towards 20 °C in steps of 10 °C at a rate of 5 °C min^{-1}. The samples were kept for 2 h under isothermal conditions after each 10 °C cooling step at this particular temperature. Annealed specimens were analyzed using the first DSC heating run at 10 K min^{-1} between −20 and 120 °C.

2.7. Tensile tests

Tensile tests were performed on a Z1.0 (Zwick-Roell, Ulm, Germany) equipped with a thermo chamber and a temperature controller (Eurotherm e2408, Limburg, Germany) using standard test specimen (ISO 527-2/1BB) at a strain rate of 5 mm min^{-1}. Stress–strain curves were recorded at ambient temperature and at T_{high} (100 °C for cPEVA20 and at 80 °C for cPEVA31). A pre-force of 50 mN was applied prior data recording. Young's modulus (E), elongation at break (ε_b) and tensile strength (σ_b) were determined. Additionally, the obtained stress–strain data at T_{high} were analyzed by Mooney–Rivlin equations for calculation of the crosslink density (ν_c) (eqn (5) and (6)) of cPEVAs.[19,20]

$$\frac{\sigma_n}{\lambda - \lambda^{-2}} = 2C_1 + \frac{2C_2}{\lambda} \quad (5)$$

$$\nu_c = \frac{2C_1}{RT} \quad (6)$$

where σ_n is the tensile stress, λ is the strain rate, $2C_1$ and $2C_2$ are the Mooney–Rivlin constants, R is the gas constant (8.314 J K^{-1} mol^{-1}), and T is the absolute temperature.

2.8. Cyclic, thermomechanical tensile tests

Testing machine and specimen dimensions were the same as described for tensile tests. Each test cycle consisted of a temperature-memory creation procedure (TMCP), where the temporary shape was created at T_{deform}, and a recovery module under stress-free conditions (see ESI Fig. S3a†). The first cycle was used as a preconditioning cycle to erase the thermo-mechanical history of the samples.

TMCP-module. The specimen was cooled from T_{high} to T_{deform} and deformed to an elongation $\varepsilon_m = 150\%$, where the strain was kept constant for 10 minutes to allow relaxation. Then the sample was cooled at 5 K min^{-1} to $T_{low} = 0$ °C and equilibrated for 10 min under strain controlled conditions. Finally, the stress was removed and the elongation of the sample in the temporary shape ε_u was determined. The deformation temperatures (T_{deform}s) in subsequent cycles were 90, 65, 40, 25, and 10 °C for cPEVA20 series and 70, 55, 40 25, and 10 °C for cPEVA31 series.

Recovery module. The recovery of the original shape was induced by heating the programmed sample to T_{high} with a heating rate of 2 K min^{-1} under stress-free conditions. After the completion of the recovery process ε_p was determined, as well as the switching temperature T_{sw}, which was obtained as inflection point in the strain–temperature recovery curve by help of first derivatives.

The extent, to which the applied deformation (ε_m) could be fixed, was quantified by the shape fixity ratio R_f, which was calculated according to eqn (7). Similarly the ability of the material to recover its original shape was quantified by the shape recovery ratio R_r using eqn (8). ESI Fig. 3a† shows the schematic illustration of the TMCP and both recovery modules in a temperature–strain–stress 3D plot.

$$R_f(N) = \frac{\varepsilon_u(N)}{\varepsilon_m} \times 100 \quad (7)$$

$$R_r(N) = \frac{\varepsilon_u(N) - \varepsilon_p(N)}{\varepsilon_u(N-1) - \varepsilon_p(N-1)} \times 100 \quad (8)$$

2.9. X-ray scattering techniques

Wide-angle X-ray scattering. WAXS measurements were performed on an X-ray diffraction system D8 discover with a two-dimensional Hi-Star detector (105 μm pixel size) from Bruker AXS (Karlsruhe, Germany). The X-ray generator was operated at a voltage of 40 kV and a current of 40 mA on a copper anode. A graphite monochromator produced Cu-K_α radiation (0.154 nm wavelength). A 3 pinhole collimator with an opening of 0.8 mm was used. The distance between sample and detector was 150 mm, calibrated with Corundum standard. *In situ* measurements during TMCP were performed using a custom-build stretching device, a heating gun, and a cooled nitrogen gas stream with 5 min exposure time per scattering pattern.

Integration of intensity *vs.* scattering angle 2θ led to one-dimensional curves for analysis. The peaks of the two phases (amorphous and crystalline) were fitted with Pearson VII functions. The crystallinity index (x_c) was determined from the areas of crystalline and amorphous peaks using eqn (9).

$$x_c = \frac{A_{cryst}}{A_{cryst} + A_{amorph}} \times 100 \quad (9)$$

The average lateral crystal size (l_c) was calculated from the (110) reflection by the Scherrer method with $k = 0.9$.[21] Integration of intensity *versus* azimuthal angle χ data led into one-dimensional curves for analysis of the degree of crystal orientation.

Small-angle X-ray scattering (SAXS). SAXS measurements were performed on a Nanostar diffractometer from Bruker AXS (Karlsruhe, Germany) equipped with a two dimensional VANTEC-2000 detector (68 μm pixel size) using a monochromatic beam with a wavelength of 0.154 nm. The distance sample to detector was 1070 mm, the beam size 400 μm. In addition SAXS

data with short exposure times were recorded at the μSpot beamline at BESSYII (Berlin, Germany) with a sample to detector distance of 810 mm and 0.15418 nm wavelength on a MAR-CCD detector (73.2 μm pixel size). Machine background weighted by the absorption factor was subtracted from the raw data. Invalid pixels (*e.g.* beam stop) were masked. The image was aligned, rotated, harmonized (assuming fiber-symmetry) and extrapolated towards high scattering vector $\mathbf{s} = (s_1, s_2, s_3)$. Thereafter, the data were projected on the fiber plane, multiplied by s^2 (Laplacian in real space), the background which occurred due to the non-ideal nature of the two-phase system was removed by spatial frequency filtering, and finally an interference function $G(s)$ was obtained. From $G(s)$ the chord distribution function CDF $z(r)$ was calculated by Fourier transformation.[22] $z(r)$ is the Laplacian of Vonk's multidimensional correlation function.[23] It visualizes size and arrangement of the nanodomains in the sample, *e.g.* long period, lamellae thickness and extension. The longitudinal long period (L) and the average crystal thickness d_c were calculated from CDF analysis.[24]

3. Results and discussion

3.1. Characterization of copolymer networks

Two series of crosslinked poly[ethylene-*co*-(vinyl acetate)] comprising two different vinyl acetate contents (VAC of 20 wt% and 31 wt%) and three different crosslink densities (achieved by crosslinking with dicumyl peroxide (DCP) weight contents of 0.5, 1, and 2 wt%), and thus providing various melting transition intervals and crystallinities, were synthesized. Samples were denoted as cPEVAxxDyy, where xx represents the vinyl acetate content (VAC) and yy the DCP wt% in the starting mixture. Gel contents with $G > 85\%$ were observed for all cPEVAs, when the DCP content was 1 and 2 wt% in the starting reaction mixture $G > 90\%$ was reached. The VAC of the copolymer networks was determined *via* thermogravimetric analysis (TGA), revealing a VAC of 20 wt% and 31 wt% for the cPEVA20 and the cPEVA31 series respectively (Table 1). Data for cPEVA20 series were adopted from ref. 15. The theoretical average segment length of polyethylene (PE) sequences (n_0) was determined from the ^{1}H-NMR spectra (ESI Fig. S1†), here $n_0 =$ 24 and 13 PE repeating units (–CH_2–CH_2–) for the cPEVA20 and the cPEVA31 series were calculated respectively.

The equilibrium degree of swelling (Q) was found to decrease from 1510% to 630% with increasing DCP content in the starting mixture. The crosslink density, as determined by Mooney–Rivlin analysis (Table 1), increased from $\nu_c = 70$ mol m^{-3} to 260 mol m^{-3} for cPEVA20 and from $\nu_c = 80$ mol m^{-3} to 325 mol m^{-3} for cPEVA31 series with increasing DCP content, which was in good correlation with the obtained Q values. The Mooney–Rivlin constant $2C_1$, which is mainly related to the number of covalent netpoints in the networks, was found to increase with increasing DCP content in the starting reaction mixture. Similarly $2C_2$, representing the contribution of physical crosslinks like entanglements, increased with increasing DCP content.

Differential scanning calorimetry (DSC) analysis was employed to investigate thermal properties of the cPEVAs. The melting and crystallization peak temperatures of the copolymer networks obtained in DSC experiments decreased with increasing VA-content from $T_m = 81$ °C to 84 °C ($T_c = 53$ °C to 57 °C) for cPEVA20s towards $T_m = 65$ °C to 68 °C ($T_c = 36$ °C to 39 °C) for the cPEVA31 series (Table 2). Data for cPEVA20 series were adopted from ref. 15. At the same time the melting temperature interval (ΔT_m) was found to decrease from $\Delta T_m \approx$ 95 °C for cPEVA20s to $\Delta T_m \approx$ 80 °C for cPEVA31s (ESI Fig. S2†), while the same trend was observed for the melting enthalpy (ΔH_m) decreasing from ΔH_m around 67 to 70 J g^{-1} (cPEVA20s) to significantly lower values of 41 to 44 J g^{-1} for the copolymer networks with lower VAC. This observation can be attributed to the shorter PE average segment length of 13 repeating units in cPEVA31 samples resulting in the formation of smaller or thinner crystals, which melt at lower temperatures. Besides the substantial impact of the VAC on the thermal properties, the variation of the crosslinking density resulted only in minor changes of the thermal characteristics, where T_c and T_m slightly decreased with increasing crosslink density, while ΔT_m and ΔH_m remained almost unchanged.

The results of the tensile tests are summarized in Table 2. At ambient temperature the elastic modulus (E) was higher for the

Table 1 Chemical composition, gel content, equilibrium swelling and degrees of crystallinity of cPEVAs[g]

Sample ID[a]	DCP [wt%]	VAC[b] [wt%]	G[c] [%]	Q[c] [%]	x_c[d] [%]	w_c[e] [%]	$2C_1$[f] [MPa]	$2C_2$[f] [MPa]	ν_e[f] [mol m^{-3}]
cPEVA20D05	0.5	20 ± 2	85 ± 1	1300 ± 10	27.4 ± 0.7	23.8	0.21 ± 0.03	0.47 ± 0.03	69 ± 9
cPEVA20D10	1	20 ± 2	92 ± 1	840 ± 10	26.8 ± 0.7	23.3	0.47 ± 0.03	0.89 ± 0.1	150 ± 10
cPEVA20D20	2	20 ± 2	96 ± 1	630 ± 10	25.1 ± 0.9	24.4	0.81 ± 0.05	1.10 ± 0.04	260 ± 15
cPEVA31D05	0.5	31 ± 2	88 ± 1	1510 ± 10	15.7 ± 1.3	15.6	0.24 ± 0.01	0.94 ± 0.09	81 ± 4
cPEVA31D10	1	31 ± 2	94 ± 1	960 ± 10	14.3 ± 0.7	15.3	0.44 ± 0.02	1.16 ± 0.1	149 ± 6
cPEVA31D20	2	31 ± 2	96 ± 1	640 ± 10	14.1 ± 2.2	14.4	0.96 ± 0.04	1.42 ± 0.11	326 ± 13

[a] The first two-digit number in sample ID was given according to the experimental value of VA-contents in cPEVAs determined by TGA measurements and the last two-digit number was given according to the content of DCP in wt% in crosslinking reaction. [b] VA-contents in cPEVAs determined by TGA measurements. [c] Gel content G and degree of swelling Q of cPEVAs was determined in toluene at 50 °C. [d] Crystallinity index as calculated from WAXS. [e] Weight crystallinity as calculated from DSC measurements. [f] Mooney–Rivlin constants $2C_1$ and $2C_2$ and crosslink density (ν_c) were obtained based on the results of tensile tests at $T_{high} > T_m$ according to Mooney–Rivlin equations. [g] Data of cPEVA20 series were adopted from ref. 15.

Table 2 Thermal and mechanical properties of cPEVAs[c]

				Ambient temperature[b]			T_{high}[b]		
Sample ID	T_m[a] [°C]	T_c[a] [°C]	ΔH_m[a] [J g^{-1}]	E [MPa]	σ_b [MPa]	ε_b [%]	E [MPa]	σ_b [MPa]	ε_b [%]
cPEVA20D05	84	57	68.3	27 ± 3	17 ± 2	700 ± 80	0.5 ± 0.1	0.8 ± 0.1	740 ± 100
cPEVA20D10	83	56	67.1	26 ± 4	17 ± 5	660 ± 50	0.7 ± 0.1	0.7 ± 0.1	380 ± 90
cPEVA20D20	81	53	70.1	28 ± 1	15 ± 1	635 ± 10	1.2 ± 0.1	0.9 ± 0.1	190 ± 50
cPEVA31D05	68	39	45.0	12 ± 1	14 ± 2	755 ± 50	0.6 ± 0.1	1.6 ± 0.1	1010 ± 50
cPEVA31D10	66	38	44.0	11 ± 1	16 ± 5	700 ± 60	1.0 ± 0.1	1.3 ± 0.1	515 ± 30
cPEVA31D20	65	36	41.2	11 ± 1	14 ± 3	615 ± 10	1.5 ± 0.1	1.1 ± 0.2	200 ± 50

[a] Data determined by DSC: melting transition temperature (T_m); crystallization temperature (T_c) and overall melting enthalpy (ΔH_m). [b] Young's modulus (E), elongation at break (ε_b), and its corresponding stress (σ_b) were determined by tensile tests at ambient temperature and at T_{high} = 100 °C for cPEVA20s and at T_{high} = 80 °C for cPEVA31s. [c] Data of cPEVA20 series were adopted from ref. 15.

cPEVA20 series (~27 MPa) than for the cPEVA31 series (~11 MPa), which was attributed to additional physical netpoints (*i.e.* PE crystals) in the cPEVA20 series, which had a higher degree of crystallinity. Elongation at break (ε_b) at ambient temperature decreased from 700% to 635% for the cPEVA20 series and from 755% to 615% for the cPEVA31 series when crosslinking density increased. As the decrease in ε_b was low, we concluded that the PE crystals as physical netpoints dominated the elastic properties. The corresponding stress at break (σ_b) was almost constant within a series, being ~16 MPa for cPEVA20s and ~14 MPa for cPEVA31s. At $T_{high} > T_m$, *i.e.* in the viscoelastic state, the mechanical properties were only influenced by the chemical crosslinks and the entanglements of the polymer chains. E increased from 0.5 to 1.2 MPa for cPEVA20s and from 0.6 to 1.5 MPa for cPEVA31s with increasing crosslink density. Also ε_b was reduced with increasing crosslink density, decreasing from 740% to 190% for cPEVA20s and from 1010% to 200% for cPEVA31s. Here a good correlation to the results from the Mooney–Rivlin analysis was observed.

The overall crystallinity determined from wide-angle X-ray scattering (x_c) or DSC (w_c) experiments was similar, being around 25% for the cPEVA20 and about 15% for the cPEVA31 series (Table 1). This observation indicates that the amount of crystals was not affected by the introduced crosslinks.

The nanostructure of cPEVAs was analyzed by small- and wide-angle X-ray scattering (SAXS and WAXS) measurements at ambient temperature. Crystallinity index (x_c) and average lateral crystal extension (l_c) were determined from the (110) reflection of PE in the WAXS pattern, while the average long period (L) and the average lamella crystal thickness (d_c) were obtained from SAXS data. The calculated results are listed in Table 3. All non-programmed samples exhibited isotropic Debye–Scherrer rings in WAXS and circular correlation rings in SAXS experiments, indicating that the crystalline domains are randomly arranged. The L and d_c were almost similar for both cPEVA series with values about $L \approx 12$ nm and $d_c \approx 6$ nm (*c.f.* Table 3). As L was found to be approximately two times d_c in cPEVAs, the crystallinity within a stack can be anticipated as ≈50%. Their structure might consist of stacks of alternating crystalline-amorphous PE lamellae, which are surrounded by a mixed amorphous PE-VA matrix comprising short PE-segments, unable to form crystals.

Based on the obtained average PE crystal thickness of 6 nm it can be assumed that the ordered PE nanostructure is related to PE segments with an average segment length of about 20 to 25 repeating units, which was in good correlation with the theoretical calculations from the NMR spectroscopy data for cPE-VA20s. For the cPEVA31 series, with a calculated average segment length of 13 repeating units, one would expect an average crystal thickness around 3 nm, but in WAXS experiments we observed also a $d_c \approx 6$ nm. This difference might be attributed to a non-statistical distribution of the VA moieties within the copolymer matrix and thus larger PE segment lengths than predicted by the theory.

As the deformation temperature T_{deform} was assumed to be the key parameter for creation of a TME in polymers, we further investigated the crystalline thickness as function of temperature exemplarily for cPEVA31D20 and cPEVA20D20. The non-deformed samples were heated in 10 K steps from 25 °C to 75 °C and SAXS patterns were recorded. In Fig. 1a and Table 3 the resulting d_c *vs.* temperature data are presented, showing a continuous increase of the crystal thickness with increasing temperature. The maximum d_cs were 8.5 nm for cPEVA20D20 at 75 °C and 7.5 nm for cPEVA31D20 at 63 °C, whereby the lower maximum d_c of cPEVA31D20 can be attributed to a lower PE-segment length.

3.2. Temperature-memory capability

The applied T_{deform}s for the TME experiments were chosen to span the whole melting temperature interval ΔT_m obtained in DSC experiments. Thus T_{deform}s for cPEVA20s ranged from 10 to 90 °C and for cPEVA31s deformation temperatures from 10 to 70 °C were utilized (for details see Experimental section). The temperature-memory capability of cPEVAs was investigated by cyclic thermomechanical tensile tests (see Scheme in ESI Fig. S3a†) and the obtained results are summarized in ESI Table S1 and S2.† The temporary shape in semi-crystalline shape-memory polymers is fixed by crystallizable

Table 3 Crystalline domain sizes and distances during TMCP as determined by SAXS/WAXS experiments

$\varepsilon = 0\%$					$\varepsilon_m = 150\%$					ε_u at T_{low} [e]				
T_{deform} [°C]	L^a [nm]	l_c^b [nm]	d_c^c [nm]	x_c^d [%]	T_{deform} [°C]	L^a [nm]	l_c^b [nm]	d_c^c [nm]	x_c^d [%]	T_{deform} [°C]	L^a [nm]	l_c^b [nm]	d_c^c [nm]	x_c^d [%]
cPEVA20D20														
25	11.4 ± 0.5	10.4 ± 0.5	6.0 ± 0.5	27 ± 2	25	12.2 ± 0.5	4.9 ± 0.5	5.9 ± 0.5	28 ± 2	25	12.6 ± 0.5	5.3 ± 0.5	5.9 ± 0.5	30 ± 2
40	12.6 ± 0.5	9.8 ± 0.5	6.5 ± 0.5	20 ± 2	40	13.2 ± 0.5	9.9 ± 0.5	5.5 ± 0.5	20 ± 2	40	11.4 ± 0.5	6.6 ± 0.5	4.3 ± 0.5	28 ± 2
65	14.9 ± 0.5	9.0 ± 0.5	7.7 ± 0.5	11 ± 2	65	18.9 ± 0.5	9.6 ± 0.5	9.0 ± 0.5	9 ± 2	65	14.3 ± 0.5	10.2 ± 0.5	6.1 ± 0.5	28 ± 2
										90	12.5 ± 0.5	10.4 ± 0.5	5.4 ± 0.5	29 ± 2
cPEVA31D20														
25	11.5 ± 0.5	6.1 ± 0.5	5.9 ± 0.5	14 ± 2	25	11.5 ± 0.5	5.2 ± 0.5	4.5 ± 0.5	15 ± 2	25	11.0 ± 0.5	6.5 ± 0.5	4.4 ± 0.5	16 ± 2
40	12.4 ± 0.5	5.2 ± 0.5	6.4 ± 0.5	12 ± 2	40	14.9 ± 0.5	5.4 ± 0.5	7.2 ± 0.5	11 ± 2	40	13.1 ± 0.5	6.0 ± 0.5	5.4 ± 0.5	14 ± 2
55	14.1 ± 0.5	4.4 ± 0.5	7.0 ± 0.5	9 ± 2	55	18.4 ± 0.5	5.4 ± 0.5	8.2 ± 0.5	7 ± 2	55	13.1 ± 0.5	6.6 ± 0.5	6.0 ± 0.5	14 ± 2
										70	12.5 ± 0.5	7.2 ± 0.5	4.8 ± 0.5	13 ± 2

[a] Long period determined from CDF. [b] Average lateral crystal extension determined from (110) reflection. [c] Average crystal thickness determined from CDF. [d] Crystallinity determined from WAXS. [e] Measurements performed at $T_{low} = 10$ °C on samples, which were deformed at T_{deform} and cooled to $T_{low} = 10$ °C to fix the temporary shape (ε_u).

Fig. 1 (a) Average lamellae thickness d_c determined by SAXS of non-deformed cPEVA20D05 (black squares) and cPEVA31D05 (open circles) during heating and theoretical prediction of the lamellae thickness (grey stars) from the peak maximum (P0 to P5) of graph b; (b) relative heat flow curves obtained in DSC experiments conducted after subsequent annealing at 90, 80, 70, 60, 50, 40, 30, and 20 °C for cPEVA20D05 (black) and cPEVA31D05 (gray); (c) DSC curves of annealed cPEVA20 with different crosslinking density, cPEVA20D05 (black), cPEVA20D10 (grey) and cPEVA20D20 (light grey) and (d) DSC thermograms of cPEVA31 samples with different crosslinking density cPEVA31D05 (black), cPEVA31D10 (grey) and cPEVA31D20 (light grey).

switching segments, which act as temporary physical netpoints. In a classical thermally-induced SME cycle the sample is deformed at $T_{high} > T_m$, where the switching segment is amorphous, and cooled to $T_{low} < T_m$ allowing crystallization of the switching segment and thus the formation of temporary netpoints which retain the temporary shape. By reheating to T_{high} the temporary netpoints are disassembled by melting of the switching segment and the permanent shape is recovered.

All investigated cPEVAs exhibited excellent temperature-memory properties demonstrated by an almost linear correlation between the T_{deform} and the response temperature T_{sw} (Fig. 2). The recorded stress–temperature–strain plots obtained under stress-free conditions are exemplarily displayed for cPEVA20D10 in ESI Fig. 3b.† The stress at ε_m was increasing when T_{deform} was decreased, which was attributed to the higher crystallinity of the sample. For equal T_{deform} the stress increased with increasing crosslink density, which was related to the additional covalent netpoints. High shape recovery ratios of $R_r \geqslant 87\%$ were achieved for all copolymers independent from the applied T_{deform}, indicating the high entropic elasticity of the polymer networks at T_{high}, reflecting the excellent stabilization of the permanent shape by the chemical crosslinks. In contrast, the shape fixity ratios were found to decrease with decreasing T_{deform} from R_f around 100% to R_f values of 50 to 60% for $T_{deform} = 10$ °C (*c.f.* Fig. 2). R_f values above 100% were attributed to crystallization induced elongation upon cooling at constant stress as previously reported.[25]

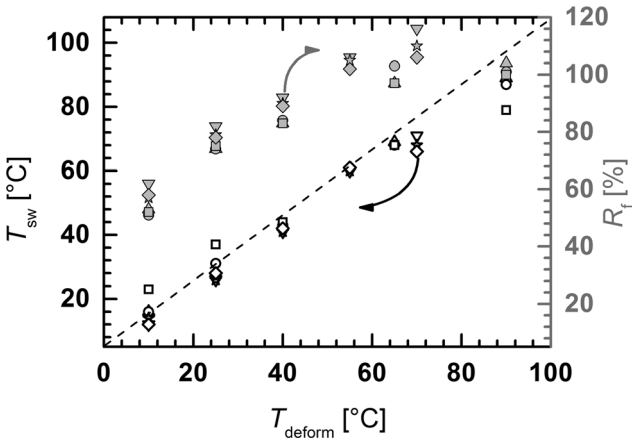

Fig. 2 Temperature-memory effect of cPEVAs. Response temperatures T_{sw} (open symbols) and shape fixity ratio R_f (solid symbols) depending on T_{deform} determined by cyclic thermomechanical tensile tests of cPEVA20D05 (triangle up), cPEVA20D10 (circle), cPEVA20D20 (square), cPEVA31D05 (triangle down), cPEVA31D10 (star), and cPEVA31D20 (diamond) as function of the deformation temperature T_{deform}. The dotted line denotes the linear correlation $T_{sw} = T_{deform}$ representing an ideal temperature-memory effect.

3.3. Annealing experiments

Annealing experiments were conducted on cPEVAs to investigate the contribution of the isothermal crystallization to the crystal structure. For doing so, non-deformed specimens were annealed stepwise in the thermo-chamber of the tensile tester and were analyzed by a first DSC heating run. The resulting thermograms are shown in Fig. 1.

As mentioned before the broad ΔT_m of cPEVAs can be treated as an infinite number of sharp single melting temperatures, whereby each individual transition would be controlled by a crystal population of a distinct thickness. Therefore, the broad ΔT_m in cPEVAs can be assumed as broad distribution of crystal lamellae thicknesses, which are related to the PE-segment length distribution. Here, the Thomson–Gibbs equation (eqn (10)) describes the relation between crystal thickness d_c and its melting temperature T_m.[26,27] Where T_m^0 is the melting temperature of an infinitely large PE-crystal (414.4 K)[28] and γ_e is the top and bottom surface energy of the crystalline lamellae (33 erg cm^{-2}).

$$T_m = T_m^0 - \frac{2\gamma_e T_m^0}{d_c \Delta H_m} \quad (10)$$

A stepwise annealing protocol, where the samples were first heated to 90 °C and then cooled to 20 °C in subsequent steps of 10 K, while allowing isothermal crystallization at each temperature, was applied to separate different crystal populations within ΔT_m from each other (see Experimental section). The annealed samples were analyzed by DSC heating experiments. In Fig. 1b the DSC curves obtained in the first heating run of cPEVA20d05 and cPEVA31D05 are shown. Both cPEVA series exhibited multiple distinct melting peaks (P0 to P4/P5) corresponding to the applied individual annealing temperatures, which was similar to the behavior reported for annealed non-crosslinked PEVA[29,30] comprising multiple T_ms. The T_ms could be related to the corresponding theoretical lamellae thickness (Fig. 1a) representing the contribution of the isothermal crystallization step during TMCP. Theoretical thickness increased from 3.9 nm for $T_m = 15$ °C to 8.3 nm for $T_m = 80$ °C, indicating the formation of thick and thermally stable crystals when increased isothermal crystallization temperature was applied. The theoretical d_c values were smaller than the d_c determined from SAXS, especially at low temperatures, because SAXS showed the average lamellae thickness with contributions from the entire crystal population. The influence of the annealing treatment on cPEVAs could be interpreted as follows: The peak P5 at 80 °C could only be observed for cPEVA20s comprising a higher PE segment length. A pronounced influence of the crosslink density on the peak area of the P4 and P5 became only apparent for cPEVA20 samples, while cPEVA31 networks were not affected by the variation of the crosslink density (Fig. 1c and d). Here the peak area of P5 was found to decrease with rising crosslink density, which can be attributed to a reduction of PE-segment length leading to the formation of thinner crystal lamellae resulting in an increase in the peak area of P4. In contrast the peaks P0, P1, P2 and P4 were not affected by increasing the crosslink density (Fig. 1c). Summarizing, higher T_{deform}, which correspond to isothermal crystallization at higher temperatures, would favor the creation of thick crystalline lamellae. In contrast lower T_{deform} would promote thin crystals. By cooling to T_{low} additional crystallization occurs in both cases but the resulting average crystal thickness would be increased when a higher T_{deform} was applied. In this way higher or lower T_{deform} will contribute to the TME.

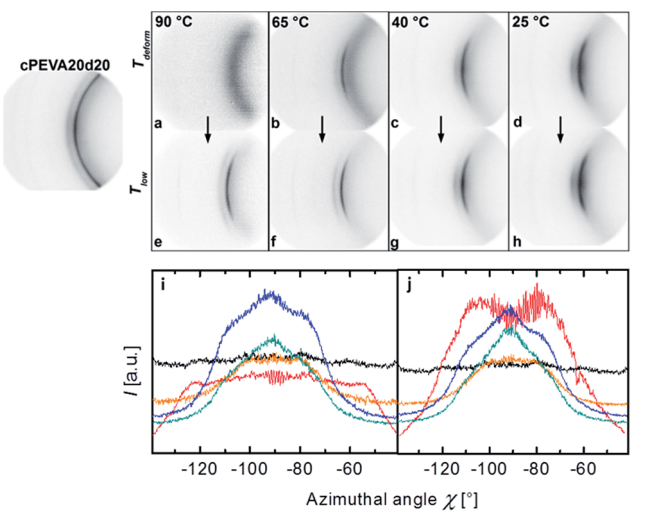

Fig. 3 Equatorial section of the wide-angle X-ray scattering patterns of cPEVA20D20 (a–h) during TMCP. Left: $T_{low} = 10$ °C and $\varepsilon = 0\%$; (a–d) at T_{deform} (as indicated) and $\varepsilon_m = 150\%$; (e–h) at $T_{low} = 10$ °C and ε_u (temporary shape); (i and j) azimuthal profiles of the (110) diffraction of cPEVA20D20 at the different situations (a–h). (i) non-deformed (black), a (red), b (orange), c (dark cyan) and d (blue); (j) non-deformed (black), e (red), f (orange), g (dark cyan) and h (blue).

3.4. Nanostructural investigations by SAXS/WAXS – mechanistic aspects of TME

In addition to the contribution of the isothermal crystallization at T_{deform}, the deformation step was expected to have significant influence on the crystal structure responsible for memorizing T_{deform}. Thus the crystalline PE nanostructures were analyzed before and after deformation at T_{deform} as well as after completion of the TMCP at T_{low}. In this way the contributions of the deformation step and the cooling step on the crystallizable controlling units responsible for the TME should be elucidated. The obtained WAXS patterns as well as the azimuthal profiles are shown in Fig. 3 for cPEVA20D20 and in ESI Fig. 4† for cPEVA31D20, while the respective SAXS patterns are displayed in Fig. 4. The analyzed structural parameters such as the degree of crystallinity (x_c), the average lateral crystal size (l_c), the average crystal thickness (d_c) and the longitudinal long period (L) calculated from SAXS and WAXS diffraction patterns are listed in Table 3. It has to be pointed out that at the highest T_{deform}s (*i.e.* 90 °C for cPEVA20D20 and 70 °C for cPEVA31D20) the specimens are amorphous as all crystals are in the molten state and in this way the TMCP and the recovery could be considered as a classical shape-memory experiment.

The illustrated WAXS patterns (Fig. 3a–h and ESI Fig. 4a–h†) represent the structures at ambient temperature before deformation, when deformed to $\varepsilon_m = 150\%$ at different T_{deform}s (cPEVA20D20: 90, 65, 40 and 25 °C; cPEVA31D20: 70, 55, 40 and 25 °C) and at $T_{low} = 10$ °C after completion of TMCP. For all samples the main ($hk0$) reflections, *i.e.* (110) and (200) were found on the equatorial part, reflecting that the orientation of the polymer chains is parallel to the strain direction. The meridional part of the pattern did not exhibit any reflections. The overall degree of crystallinity of both programmed copolymer samples was found to be similar to the original non-programmed sample with x_c in the range of 27 to 30% for cPEVA20D20 and x_c values from 13 to 16% for cPEVA31D20. With increasing T_{deform} x_c was found to systematically decrease to $x_c = 9\%$ (cPEVA20D20 at 65 °C) or 7% (cPEVA31D20 at 55 °C) while almost no difference between elongated and non-elongated test specimen could be observed, which suggested that strain-induced crystallization processes are not involved during TMCP.

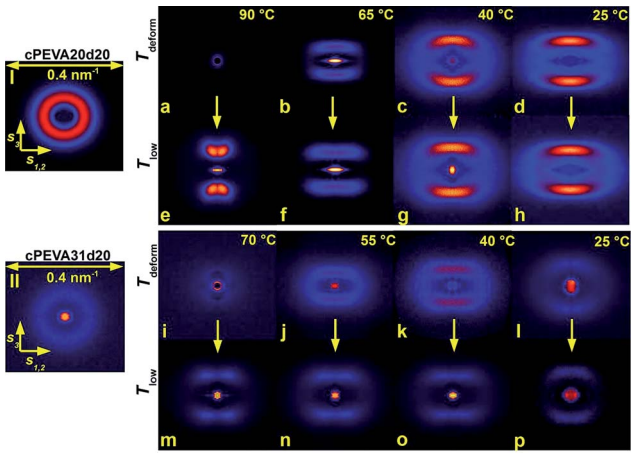

Fig. 4 SAXS patterns of cPEVA20D20 (I and a–h) and cPEVA31D20 (II and i–p) during TMCP. I and II: $T_{low} = 10$ °C and $\varepsilon = 0\%$; (a–d and i–l) T_{deform} (indicated) and $\varepsilon_m = 150\%$; (e–h and m–p) $T_{low} = 10$ °C and ε_u (temporary shape).

Different azimuthal profiles related to the (110) peak were obtained for copolymers with different VAC equivalent to a different PE segment length. Here cPEVA20D20 (Fig. 3) showed a lower degree of orientation compared to cPEVA31D20 (ESI Fig. 4†), which exhibited sharper peak profiles (χ direction), which were attributed to a higher mobility of smaller crystals and therefore a higher orientation after application of the deformation. A broadening of the azimuthal profiles in χ direction was observed with increasing T_{deform}. Interestingly at $T_{deform} = 90$ °C a somehow bimodal azimuthal profile was observed, which might be attributed to a structure of tilted lamellae.[31]

The average lateral crystal size (l_c) determined from the (110) reflection of the programmed cPEVA20D20 samples at ambient temperature was found to increase from $l_c = 5.3$ nm to $l_c = 10.4$ nm with increasing T_{deform} from 25 °C to 90 °C. The samples programmed at higher T_{deform}s of 90 °C and 65 °C exhibited a similar l_c around 10 nm like the original non-programmed sample. This leads to the conclusion that at high T_{deform}, where only a few or almost no PE crystals are present after deformation, the crystal growth during cooling to T_{low} is not hindered and larger crystals can be formed. Significantly lower l_c values in the range of 5 to 7 nm were found at lower deformation temperatures. This might be explained by the disruption of existing PE crystals into smaller microfibril-like structures during the deformation at lower T_{deform}. The new crystalline structures formed during further cooling to T_{low} are hindered in extension by the small structures generated during deformation, which resulted in an overall reduction of the lateral extension of the crystalline domains. Similar findings have been reported for a cold drawn polyethylene-octene copolymer.[32]

In contrast for cPEVA31D20 having a lower PE segment length the l_c-values remained almost constant around 6 to 7 nm independent from the applied T_{deform}, which corresponds to the l_c of the non-programmed sample.

In addition to the crystallinity and the lateral crystal size data, the *in situ* SAXS experiments provide information about the longitudinal long period L, including one amorphous and one crystalline layer, and the average thickness of the crystalline lamella d_c. In Fig. 4 various SAXS patterns obtained for the original non-deformed cPEVA20D20 and cPEVA31D20 sample at ambient temperature (Fig. 4I and II), at different T_{deform} with $\varepsilon_m = 150\%$ (Fig. 4a–d and i–l) and after completion of TMCP at T_{low} (Fig. 4e–h and m–p) are shown. Both non-programmed samples cPEVA20D20 and cPEVA31D20 exhibited an isotropic structure with a long period around $L = 11.5$ nm and a crystalline thickness of $d_c \approx 6.0$ nm. At the desired deformation temperatures without elongating the sample the isotropic structure remained and the values for L and d_c increased with raising temperature, while at $T_{deform} = 90$ °C (cPEVA20D20) and at $T_{deform} = 70$ °C (cPEVA31D20) no discrete scattering pattern could be observed.

In the following first the further SAXS data obtained for cPEVA20D20 will be discussed. Also after deformation to ε_m = 150% at T_{deform} = 90 °C no discrete scattering pattern could be observed, while after cooling to T_{low} and releasing the stress in the temporary shape a four point pattern was obtained (Fig. 4e). This pattern exhibits a typical correlation in the s_3 direction of elongation, which can be attributed to a structure of tilted lamellae. When lower T_{deform}s of 65, 40 and 25 °C were applied the SAXS patterns achieved during deformation at T_{deform} and after completion of TMCP differed strongly from those obtained at 90 °C. Here a relatively broad lateral distribution of the maxima was generated with patterns having a distinct streak parallel to the equator ($s_{1,2}$), which indicate a microfibrillar or cylinder-like structure.[33] Such a transformation from the point reflections in the non-deformed state to a microfibrillar or cylinder-like structure can be attributed to inter- and intra-lamellar slipping processes and crystallite fragmentation during deformation at low T_{deform}s.[34]

The SAXS pattern obtained for cPEVA31D20, with exception of T_{deform} = 70 °C, where the sample was completely amorphous, had a four-point character similar to cPEVA20D20 (Fig. 4i–p), whereby these pattern appear more layer-like, which can be attributed to a pronounced cylinder-like structure of the crystalline PE domains.

Programming at T_{deform} = 90 °C, where the copolymer network is completely amorphous, resulted in similar values for the long period (L = 12.5 nm) and the crystalline thickness (d_c = 5.4 nm) as in the original state. Here, the cooling to T_{low} = 10 °C generated a subsequent increasing population of crystalline domains, starting with the formation of thicker crystals at higher temperatures and ending with thinner crystals at lower temperatures, which are placed in between the previously formed ones. A similar trend was observed when the sample was deformed at T_{deform} = 65 °C, where a crystalline fraction of x_c = 9% remained and a L of 18.9 nm and a d_c of 9.0 nm represented the existing PE crystals. After cooling to T_{low} the long period as well as the average crystal thickness decreased to L = 14.3 nm and d_c of 6.1 nm, respectively.

After deformation at lower T_{deform}s of 40 °C and 25 °C long periods of L = 13.2 nm and L = 12.2 were obtained, which are slightly higher compared to the values observed for the non-deformed samples at the same T_{deform}s, whereas the crystal thickness was reduced to values of 5.5 to 5.9 nm. After cooling from T_{deform} = 40 °C to T_{low} both the longitudinal long period and the crystal thickness were found to be slightly reduced to L = 11.4 nm and d_c = 4.3 nm. Together with the increase in x_c and the decrease in l_c obtained from WAXS experiments this indicated that less laterally extended crystals are intersected between the existing crystalline domains. When programmed at 25 °C L and d_c were not affected during cooling to T_{low} = 10 °C, while x_c increased substantially, which indicated that a small fraction of identical crystalline structures were inserted in between existing crystals upon cooling.

During programming at lower T_{deform}s the predominant process was the structural rearrangement of existing PE crystallites, which was dictated by the deformation.

A similar trend for the changes in the crystalline nanostructure was observed for cPEVA31D20 when programmed at higher T_{deform}s of 70, 55 or lower T_{deform}s of 40 and 25 °C, but less pronounced (see Table 3).

Based on the observations from WAXS/SAXS and annealing experiments two different contributions to the nanostructural changes in cPEVA responsible for the memorization of the deformation temperature depending on the choice of T_{deform} were proposed, which are schematically displayed in Fig. 5. Starting from the non-deformed sample with a broad distribution of crystal thickness as reflected by its broad melting transition (DSC results), heating to higher T_{deform} (Fig. 5a–e) results in a few remaining thicker crystals, which are thermally stable at these temperatures, as confirmed by SAXS measurements. Annealing at this T_{deform} increased the thermally stable crystal fraction. When the deformation is applied these crystals are tilted and oriented, whereby some crystal thickening might occur. By cooling to T_{low}, oriented PE chains crystallize and finally relatively thick crystals are generated. The now established nanostructure of the temporary shape has a broader crystal thickness distribution compared to the starting structure. In order to induce the TME by reheating, higher temperatures need to be exceeded to melt these thicker crystals and in this way the sample remembers the higher T_{deform}.

At lower T_{deform}s (Fig. 5a–e') the overall starting nanostructure is almost maintained during the initial heating step as only a few thinner crystals are melting. Annealing at low temperatures would increase the thermally less stable crystal fraction. When the deformation is applied, rearrangement of the nanostructure takes place in such way that thicker and larger crystals were disrupted into smaller and thinner (and less lateral extended) ones, which are oriented. By cooling to T_{low} = 10 °C only a few thinner crystals can grow as the space for crystallization is already occupied. Finally, the temporary shape comprises a nanostructure with thin and small oriented crystals, which melt at low temperatures during reheating and in this way the sample remembers the lower T_{deform} applied during programming.

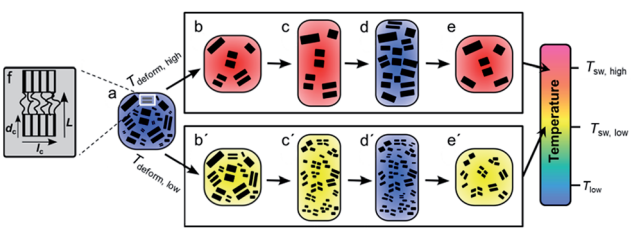

Fig. 5 Schematic illustration of the TME mechanism. Black structures represent crystalline domains of different size. The upper pathway (b to e) shows the mechanism for higher $T_{deform,high}$ and the lower pathway (b′ to e′) for lower $T_{deform,low}$. Furthermore a sketch of the average crystal thickness (d_c), the average lateral extension (l_c), and the long period (L) is presented (f).

4. Conclusions

Series of cPEVAs with two different VACs comprising a broad melting temperature range and three different crosslink densities were prepared, which exhibited a pronounced temperature-memory effect. The contribution of the temperature applied during TMCP was explored by annealing experiments, which revealed preferential formation of thick crystals when higher temperatures were applied. *In situ* X-ray investigations were employed to investigate the nanostructural changes of the crystallizable PE controlling units during functionalization and activation of the temperature-memory effect, especially regarding the contribution of the deformation step. It could be shown that two different mechanisms are responsible for memorizing higher or lower T_{deform}. At higher T_{deform}s predominantly newly formed large crystal structures were established during cooling to T_{low}, which are controlling the TME. In contrast, at lower T_{deform}s, which is comparable to a cold drawing scenario, the TME was determined by the rearrangement of existing crystalline structures during deformation, whereby large crystalline structures are disrupted into smaller ones related to low response temperatures. The observed nanostructural changes during TMCP were found to be almost independent from the composition of the investigated cPEVAs. The mechanism of the TME in semi-crystalline cPEVAs with contributions from thermal treatment and mechanical deformation might be extended to other TMPs comprising crystallizable controlling units and in this way enable a knowledge based design.

Notes and references

1 P. Miaudet, A. Derre, M. Maugey, C. Zakri, P. M. Piccione, R. Inoubli and P. Poulin, *Science*, 2007, **318**, 1294–1296.
2 H. A. Khonakdar, S. H. Jafari, S. Rasouli, J. Morshedian and H. Abedini, *Macromol. Theory Simul.*, 2007, **16**, 43–52.
3 J. Cui, K. Kratz and A. Lendlein, *Smart Mater. Struct.*, 2010, **19**, 065019.
4 K. Kratz, S. A. Madbouly, W. Wagermaier and A. Lendlein, *Adv. Mater.*, 2011, **23**, 4058–4062.
5 T. Xie, K. A. Page and S. A. Eastman, *Adv. Funct. Mater.*, 2011, **21**, 2057–2066.
6 K. Kratz, U. Voigt and A. Lendlein, *Adv. Funct. Mater.*, 2012, **22**, 3057–3065.
7 D. M. Feldkamp and I. A. Rousseau, *Macromol. Mater. Eng.*, 2010, **295**, 726–734.
8 M. Y. Razzaq, M. Behl and A. Lendlein, *Adv. Funct. Mater.*, 2012, **22**, 184–191.
9 T. Xie, *Nature*, 2010, **464**, 267–270.
10 I. S. Kolesov and H.-J. Radusch, *eXPRESS Polym. Lett.*, 2008, **2**, 461–473.
11 J. Li, T. Liu, S. Xia, Y. Pan, Z. Zheng, X. Ding and Y. Peng, *J. Mater. Chem.*, 2011, **21**, 12213–12217.
12 Q. Zhang, S. Song, J. Feng and P. Wu, *J. Mater. Chem.*, 2012, **22**, 24776–24782.
13 L. Sun and W. M. Huang, *Soft Matter*, 2010, **6**, 4403–4406.
14 M. Heuchel, T. Sauter, K. Kratz and A. Lendlein, *J. Polym. Sci., Part B: Polym. Phys.*, 2013, **51**, 621–637.
15 U. Nöchel, U. N. Kumar, K. Wang, K. Kratz, M. Behl and A. Lendlein, *Macromol. Chem. Phys.*, 2014, **215**, 2446–2456.
16 W. W. Zhao, X. G. Zhong, L. Yu, Y. F. Zhang and J. Z. Sun, *Polymer*, 1994, **35**, 3348–3350.
17 H. N. Sung and J. H. Noggle, *J. Polym. Sci., Polym. Phys. Ed.*, 1981, **19**, 1593–1602.
18 *Polymer Handbook*, ed. J. Brandrup and E. H. Immergut, Wiley Interscience, New York, Chicester, Brisbane, Toronto, Singapore, 3rd edn, 1989.
19 M. Mooney, *J. Appl. Phys.*, 1940, **11**, 582–592.
20 N. Sombatsompop, *Polym.-Plast. Technol. Eng.*, 1998, **37**, 333–349.
21 A. L. Patterson, *Phys. Rev.*, 1939, **56**, 978–981.
22 N. Stribeck, *J. Appl. Crystallogr.*, 2001, **34**, 496–503.
23 C. G. Vonk, *Colloid Polym. Sci.*, 1979, **257**, 1021–1032.
24 N. Stribeck, E. Buzdugan, P. Ghioca, S. Serban and R. Gehrke, *Macromol. Chem. Phys.*, 2002, **203**, 636–644.
25 R. Alamo, R. Domszy and L. Mandelkern, *J. Phys. Chem.*, 1984, **88**, 6587–6595.
26 Q. Jiang, C. C. Yang and J. C. Li, *Macromol. Theory Simul.*, 2003, **12**, 57–60.
27 B. Wunderlich and G. Czornyj, *Macromolecules*, 1977, **10**, 906–913.
28 G. W. H. Höhne, *Polymer*, 2002, **43**, 4689–4698.
29 M. Y. Keating and E. F. McCord, *Thermochim. Acta*, 1994, **243**, 129–145.
30 X. Shi, J. Jin, S. Chen and J. Zhang, *J. Appl. Polym. Sci.*, 2009, **113**, 2863–2871.
31 N. S. Murthy and D. T. Grubb, *J. Polym. Sci., Part B: Polym. Phys.*, 2006, **44**, 1277–1286.
32 N. Stribeck, R. Androsch and S. S. Funari, *Macromol. Chem. Phys.*, 2003, **204**, 1202–1216.
33 R. Androsch, N. Stribeck, T. Lüpke and S. S. Funari, *J. Polym. Sci., Part B: Polym. Phys.*, 2002, **40**, 1919–1930.
34 S. Hobeika, Y. Men and G. Strobl, *Macromolecules*, 2000, **33**, 1827–1833.